

Design of alumina/ β -eucryptite composite from alum sludge waste: physical properties, phase composition and coefficient of thermal expansion

R. M. Khattab¹, W. H. Hegazy^{2*}, M. E. Sebak³, H. H. Abo-almaged¹

¹ Refractories, Ceramics and Building Materials Department, National Research Centre (NRC), Dokki 12622, Cairo, Egypt

² Department of Chemistry, Faculty of Science, Suez University, Suez 43533, Egypt

³ Petroleum Medical Centre, Suez, Egypt

ARTICLE INFO

Article history:

Received 17 February 2023

Received in revised form 2 March 2023

Accepted 4 March 2023

Available online 5 March 2023

Keywords

Waste materials,
Alumina,
 β -eucryptite,
thermal expansion coefficient,
alum sludge waste.

ABSTRACT

The main objective of this research is to design alumina/ β -eucryptite composite with a low coefficient of thermal expansion (CTE) and then test its sinterability using alum sludge from water treatment plants as an alumina source. A suitable chemical method is used to extract alumina from alum sludge waste. In addition to extracted alumina, silica fume waste and lithium carbonate were used to prepare β -eucryptite. In order to prepare β -eucryptite, the phase formation is first to be adjusted. The prepared samples were fired at 800, 1000, and 1200 °C, respectively. XRD, SEM, physical properties, and thermal expansion are used to characterize these samples. The results indicate that 1000°C is the optimum temperature for eucryptite formation. The samples of alumina/ β -eucryptite containing 10, 20, 30, and 40% eucryptite are then prepared, and the influence of the heat treatment on the prepared composites is studied at temperature ranges of 1300, 1400, and 1500°C. XRD analysis, microstructure, physical, and mechanical properties of alumina/ β -eucryptite composites are investigated. The coefficient of thermal expansion (CTE) for various alumina/ β -eucryptite samples at 1500°C reduces with increasing β -eucryptite content, reaching $0.8098 \times 10^{-6} \text{ }^\circ\text{C}^{-1}$. The results demonstrate that a composite with good mechanical properties and a low thermal expansion coefficient can be formed and utilized in a variety of different applications.

1. Introduction

Global recycling awareness has increased over the past ten years, and secondary industrial waste pollutants are frequently converted to renewable materials. Instead of disposing of pollutants in traditional ways, various types of recycling can help preserve materials while also reducing greenhouse gas emissions as well as the use of raw materials [1].

A wide range of waste types from various sectors of industry (for example, metallurgical, mining, and chemical waste). There is a substantial amount of secondary raw material that could be applied to a variety of different products, such as construction or pigment production. They are frequently used in industrial furnaces as refractory materials and as heat exchangers in gas turbines.

As a result, a wide range of industrial wastes have been investigated for this purpose, including metal-rich sludge's like silica fume, alumina sludge, and fly ash as sources for silica and alumina for solid state manufacturing of composite materials, all of which contaminate and harm the environment [2-4].

The primary goal of recycling is to achieve environmental sustainability by replacing raw material inputs and redirecting waste outputs such as alum sludge and silica fume outside of the economic system [2].

Coagulation-flocculation techniques are commonly used in traditional water treatment plants (WTPs) to remove suspended particles and colloids from raw water. Coagulation, flocculation, sedimentation, filtration, and disinfection are all phases of the WTPs. Aluminum sulphate ($\text{Al}_2(\text{SO}_4)_3$), also known as alum, is the coagulant in this WTP. This is due to the ease with which alum hydrolyzes in water to produce neutral alum hydroxide, from which the colloid settles into precipitated hydroxide. When the coagulant $\text{Al}_2(\text{SO}_4)_3$ is used in a water treatment process, the resulting sludge contains aluminum and is known as alum sludge [5-8]. Disposing of alum sludge in rivers, streams, ponds, lakes, drains, or landfills is not an environmentally friendly alternative. The sludge has the potential to endanger human health and disturb river biota.

The major components in all sludge samples are SiO_2 , Al_2O_3 , and Fe_2O_3 [9], which have a high selective adsorption capacity in water for particular anions [10]. The solid waste can be recovered and turned into pure aluminum compounds, which is one of the key goals of the

* Corresponding author at Suez University

E-mail addresses: whchemistry@hotmail.com (W. H. Hegazy)

study's alum sludge recycling method. The accumulation of huge amounts of solid waste that can be utilized for a variety of purposes has become a source of environmental concern, particularly in the construction industry, ceramics, and pigment manufacturing [11-13].

Alumina ceramic is a monophasic polycrystalline type of industrial sapphire that is highly oxidized, hard, and stable. Alumina has some properties in common with other polycrystalline ceramic materials, like bending resistance and moderate tensile strength, as well as brittle fracture behavior, which is the main disadvantage of alumina. Alumina is an ionic/covalent solid that, unlike metals and alloys, does not yield under load. The strong bonds in alumina are the main source of several of its characteristics, including low thermal and electrical conductivity, high melting point that makes casting alumina almost impossible, and high hardness that set apart this material and makes machining it difficult and expensive. Scientists are most concerned with alumina brittleness while constructing alumina components. Cracking energy is released in metals by resulting at the crack tip, but components of alumina can fracture without prior plastic deformation at high tensile stresses, such as notches, surface defects, internal faults, or when thermal shocks occur. Furthermore, because poly-crystalline ceramics contain a number of faults characterized by high size scatter and random position inside the solid body, some statistical analysis correlates stress distribution, failure probability, and strength in ceramics is required [14-15].

Silica fume is a pi-product of the ferro-silicon alloy and manufacturing of silicon industries; silica fume is obtained by reduction of quartz at high temperatures. To eliminate oxygen, high purity quartz is heated in an electric arc furnace with coal, coke, or wood chips at a temperature of 2000 °C. After quartz is reduced to alloy, silicon monoxide vapor is emitted and then collected at the furnace base. In the upper parts of the furnace, the fume oxidizes and intensifies, forming microspheres of un-crystalline silica, which is silicon oxide. It is an ultra fine powder, known as micro-silica, which contains 75% silicon and 85–95% non-crystalline silica [16-17].

The goal of this research is the extraction of alumina from sludge waste, according to R. M. Khattab et al. [18] to use it with silica fume approach to make an alumina-eucryptite ceramic composite.

β -eucryptite (LiAlSiO_4) has gotten a lot of attention from both industry and academia due to its shrinkage negative coefficient of thermal expansion and one-dimensional Li-ion conductivity. The β -eucryptite is a hexagonal quartz structure, in which half of the Si^{4+} ions are replaced by trivalent aluminum ions. The incorporation of mono valent lithium ions in the $(\text{Si}, \text{Al})\text{O}_4$ framework neutralizing the charge [11]. Its thermal expansion coefficients (CTE) are highly isotropic (α : $7.26 \times 10^{-6} \text{ deg}^{-1}$; γ : $-16.35 \times 10^{-6} \text{ deg}^{-1}$) [19]. As a consequence, the volume thermal expansion of the ceramics is low [20].

It has been found that solid-phase reactions are used to synthesize lithium alumino-silicate from chemically pure

materials; β -eucryptite is formed at temperatures of 1200-1250°C and does not decompose as the temperature is raised to 1400°C. In addition, lithium carbonate, quartz sand, and kaolin were used to synthesis materials [21, 22] with oxide ratios similar to β -eucryptite (LS-4) synthesis. Ceramic materials with the composition $\text{Li}_2\text{O}-\text{MgO}-\text{Al}_2\text{O}_3-\text{SiO}_2$ not only have high thermal shock resistance, but also good mechanical and dielectric properties [23-32].

In the present study, we will show the ability to design an alumina/ β -eucryptite composite from waste materials. The main objective of this research is to design a composite with a very low coefficient of thermal expansion (CTE) and test its sinterability. Composite materials were prepared using alumina (Al_2O_3) extracted from alum sludge waste using a chemical treatment method to prepare corundum separately and then included it during β -eucryptite preparation. Silica fume waste as a source of silica and lithium carbonate were used beside extracted alumina to obtain β -eucryptite. The phase composition, microstructure, mechanical, and physical properties of alumina/ β -eucryptite composites are studied at different temperatures.

2. Material and Experimental procedures

Alum sludge was collected from the Suez Canal water station (Suez, Egypt) and investigated by X-ray fluorescence (XRF). According to Table 1,

Table 1: X-ray fluorescence chemical analysis of alum sludge (XRF)

Main constituents	Wt %	Main constituents	Wt %
SiO_2	36.81	Na_2O	0.44
TiO_2	0.69	K_2O	0.58
Al_2O_3	20.84	P_2O_5	0.68
Fe_2O_3	6.46	SO_3	1.30
MgO	1.80	Cl	0.27
CaO	2.90	LOI	26.66

2.1 Extraction of alumina from alum sludge using a chemical treatment method

The alum sludge is dried at 110°C after filtration using a suction pump. The amount of final extracted alumina following fire at various temperatures was measured using chemical treatment methods based on pH. The chemical treatment procedure uses NaOH and ammonium acetate as starting components to optimize the pH for aluminum hydroxide precipitation. The extraction and characterization of alumina from alum sludge were carried out according to R.M. Khattab et al. [18, 33] as follow: mix in 66.6 g alum sludge, 30 mL sulfuric acid solution (5.647 mol/L), and distilled water until the solution mixture reaches 100 mL. All of the content was put in a 500-mL flask with a magnetic stirrer and a temperature controller and filled with the mixture. The reactants were heated at 170°C for 1 hour and agitated with a mechanical agitator at 300 rpm. After

that, 100 mL of distilled water was added to the flask, which was then kept at ambient temperature overnight to remove any soluble compounds from the resulting mixture. Following filtration of the slurry, a constant rate (3 mL/min) of sodium hydroxide solution (8.07 mol/L) was gradually added to the filtrate while stirring until pH 12 was reached. In order to completely separate $\text{Fe}(\text{OH})_3$ from soluble Al compounds, the flask was kept at room temperature overnight, and the slurry was then filtered. After a thorough washing with distilled water, the solid components with a reddish-brown color were dried in an oven at 100°C for 24 hours. The filtrate was then adjusted at 70°C with 2.194 mol/L ammonium acetate at a continuous rate of 3 mL/min., re-precipitate $\text{Al}(\text{OH})_3$ at pH 8, after extraction of $\text{Fe}(\text{OH})_3$ with NaOH. The powders are then calcined at 1400 °C to form the corundum phase. The physical characterizations of extracted aluminum hydroxide from the alum sludge show that alpha alumina was obtained at 1400°C after treatment by NaOH followed by ammonium acetate as a precipitating agent for $\text{Al}(\text{OH})_3$. Alpha alumina with nano sizes of 1-20 nm and average particle sizes ranging from 50–200 nm was obtained after heat treatment at 1400°C.

2.2 Preparation of β -eucryptite $\text{Li}_2\text{O} \cdot \text{Al}_2\text{O}_3 \cdot 2\text{SiO}_2$

Lithium carbonate, silica fume as a silica source, and alumina from the alum sludge treatment are used to prepare β -eucryptite. In a porcelain mortar, silica fume, lithium carbonate, and alumina powder (after optimizing the calcination) were mixed. The resultant powder of β -eucryptite was calcined at 800, 1000, and 1200°C, depending on the X-ray diffraction.

2.3 Preparation of alumina/ β -eucryptite composite

The preparation of alumina/ β -eucryptite is carried out in this section. After optimizing the calcination temperature of alumina and β -eucryptite (calcinated at 1000°C), four alumina/ β -eucryptite composites containing 10, 20, 30, and 40 Wt.% β -eucryptite were produced and defined as AE1, AE2, AE3, and AE4, respectively. In a roller mill, the four prepared composites are mixed before being pressed at 100 MPa and sintered at three various temperatures: 1300, 1400, and 1500°C.

2.4 Characterization

The powders calcined at 800, 1000, and 1200 °C as well as sintered composites were subjected to X-ray diffraction analysis using a Bruker D8 apparatus and CuK radiation at a scanning rate of 1 degree /minute. The microstructure of the calcined and sintered samples was studied using a scanning electron microscope (SEM-Philips XL 30). Moreover, the Archimedes water displacement method (ASTM C373-88) was used to calculate the apparent porosity and bulk density. By using a hydraulic testing device with a maximum loading capacity of 600 KN, model Seidner, Riedlinger (Germany), the compressive strength of the fired specimens was assessed. Using

rectangular bars and an automatic Netzsch DIL402 PC (Germany) dilatometer, the thermal expansion of composites sintered in the optimum temperature range of 30°C to 1000°C was measured. The heating rate used was 5 K/min.

3. Results and Discussion

3.1 X-ray diffraction of β -eucryptite

X-ray diffractions of β -eucryptite synthesized from extracted alumina from alum sludge, lithium carbonate and silica fume are shown in Fig. 1.

It is found that the increase in thermal treatment is more effective for β -eucryptite formation. Temperatures near 800°C have been reported for the formation of β -eucryptite (LiAlSiO_4) [34-35]. It was noted that modest amounts of cristobalite were present at 800 and 1000°C the primary peaks of β -eucryptite (PDF#12-0709). As the sintering temperatures rise, its intensity peaks grow. As evidenced by early increases in the intensity of β -eucryptite crystal primary diffraction peaks with increasing sintering temperature [36], the percentage content of β -eucryptite crystal increases with increasing sintering temperature. At 1200°C, β -spodumene phase is presented with β -eucryptite crystals. This result is due to the phase transformation of some of beta eucryptite to beta spodumene at high temperature.

As it is known that β -eucryptite is thermally unstable after prolong soaking time [37]. At temperatures below 900°C, the crystalline phase of β -eucryptite would form, whereas at temperatures above 900°C, β -spodumene would form [38-40]. Depending of the method used to heat treat LAS glass-ceramic, similar structures can have different properties. The peak locations of the crystal phases of β -spodumene [41-51] and β -eucryptite [52] were close to 26°, which was also generally in agreement with other researchers' findings. It was discovered that the second phase of the crystal, virgilite ($\text{LiAlSi}_2\text{O}_6$), could be generated at either a lower [48] or higher [53] soaking temperature before it changed into β -spodumene. Although the transformation of β -spodumene occurs at higher temperatures, the creation of the crystal phase also had a significant impact on how long the mixture was allowed to soak.

This is supported by additional research using a solid-state technique [41], where LAS glass-ceramic tests were carried out by altering the soaking temperature for 24 hours, although the crystalline phase only manifested at 710°C. The LAS glass-ceramic sample, meanwhile, was fired at 740 °C over the course of 24 hours, with the crystalline phase only beginning to manifest itself after 4 hours [41]. This suggests that the length of the soak had an impact on the development of the crystalline phase. To make β -spodumene of LAS glass-ceramic, more time must be spent soaking the material at lower temperatures and vice versa.

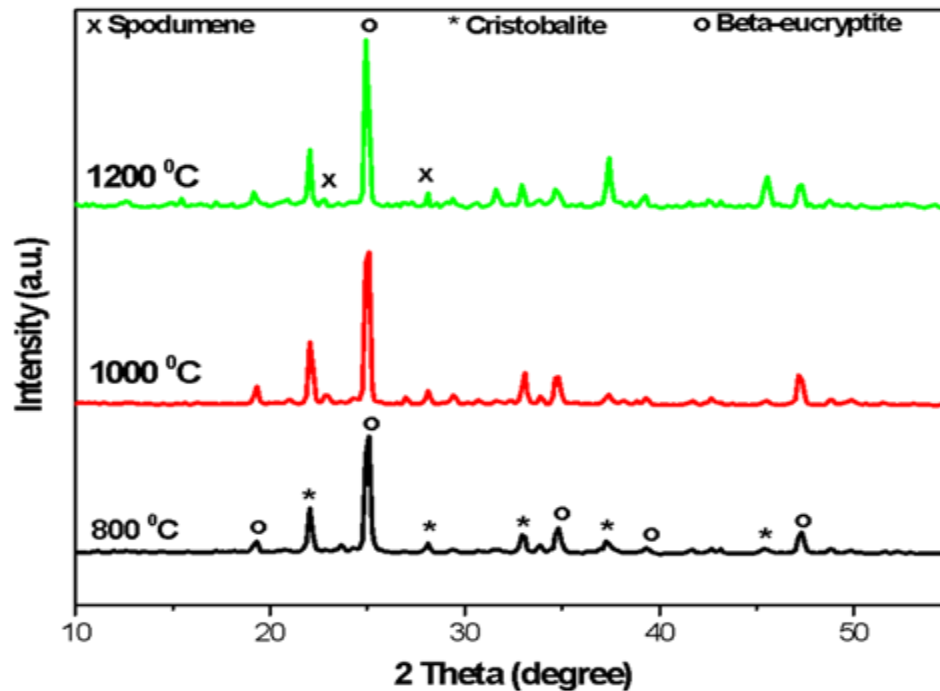


Fig. 1: XRD of β -eucryptite sintered at different temperature

3.2. SEM analysis of β -eucryptite

Fig. 2 displays the SEM images of sintered ceramics sintered at various temperatures. At 800°C, it was discovered that the abundance of glass phases in the β -eucryptite ceramics made it challenging to observe the dispersion of grains. As the sintering temperature rises, the porosity number in the ceramic sample of β -eucryptite drops. Small porosity can be seen in β -eucryptite ceramics sintered at 1200°C. Additionally, β -eucryptite appeared as a tridimensional structure made up of light grey particles that melded together. β -eucryptite is evenly disseminated in the matrix, with average particle sizes ranging from 10 to 5 μm as seen at 800 and 1000°C. Upon increasing the temperature at 1200, cubic plated shape of spodumene appeared beside β -eucryptite. It is randomly dispersed between β -eucryptite particles. In addition, the microcracks are shown at this sintered temperature. This is due to the β -eucryptite crystal structure's high anisotropy, which causes the c axis to contract while the a and b axes expand. Internal stresses are generated as a result of spontaneous grain breakup and microcrack formation [53].

3.3 Physical properties of sintered β -eucryptite samples

The bulk density and apparent porosity of fired samples at various temperatures, 800, 1000 and 1200°C are shown in Fig.3. It was observed that the apparent porosity decreases and bulk density increases with increasing the sintering temperature up to 1000°C. Then the decrease in the bulk densities was observed at 1200°C. The increase in densification parameters is due to a decrease in the viscous flow mechanism, which allows for proper sintering and hence complete densification. The density is lower at 1200°C due to the formation of

microcracks and spodumene, which have a density of about 2.4 g/cm³ [37] compared to β -eucryptite (2.65 g/cm³) [54].

In addition, another estimation for decreasing the density at 1200°C is related to Low *et al.* [55, 56] and Kobayashi *et al.* [57], who found that, additions of 20-90 Wt% spodumene resulted in decreased density due to the formation of 5–10 mm pores induced by the excess liquid phase and the less dense spodumene phase. The low porosity obtained at 1200°C is due to the spodumene liquid phase serving to decrease apparent porosity [55]. In general, during the sintering at high temperatures, the surface energy of individual particles contacts one another, forming necking between them, forming grains and reducing the empty spaces of pores. The continuous growth of grains causes grain boundary formation, which densifies and eliminates the pores [37, 54].

3.4. Thermal expansion measurement of β -eucryptite

Figure 4 depicts the relative length changes of β -eucryptite ceramics from room temperature to 1000°C for samples sintered at various temperatures (800, 1000, and 1200 °C). It can be seen that the entire curve takes the U-Shapes. For the sample sintered at 800°C. Two stages of shrinkage are seen on the linear expansion curve, one from 0 to 400 °C and another from 580 °C to 800 °C. The change of beta eucryptite thermal expansion on its crystal structure is directly related to the change of structure with temperature [53, 58-60]. Figure 4 depicts schematic diagrams of the β -eucryptite structure plan and profile. The β -eucryptite structure includes tetrahedron and octahedron structures. Li atoms are capable of occupying sites surrounded by tetrahedral or octahedral structures.

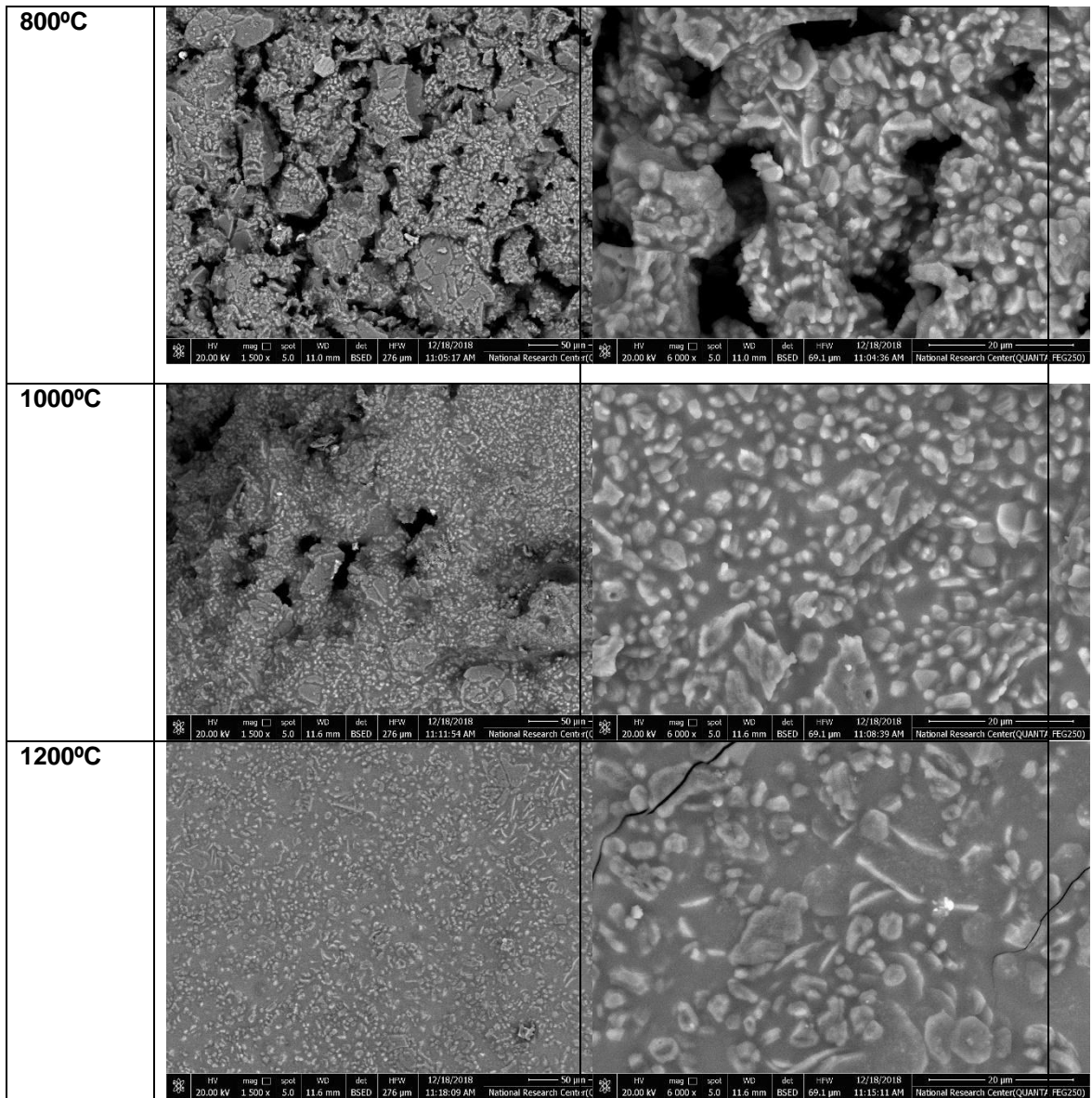


Fig. 2: SEM images of β -eucryptite sintered at different temperatures

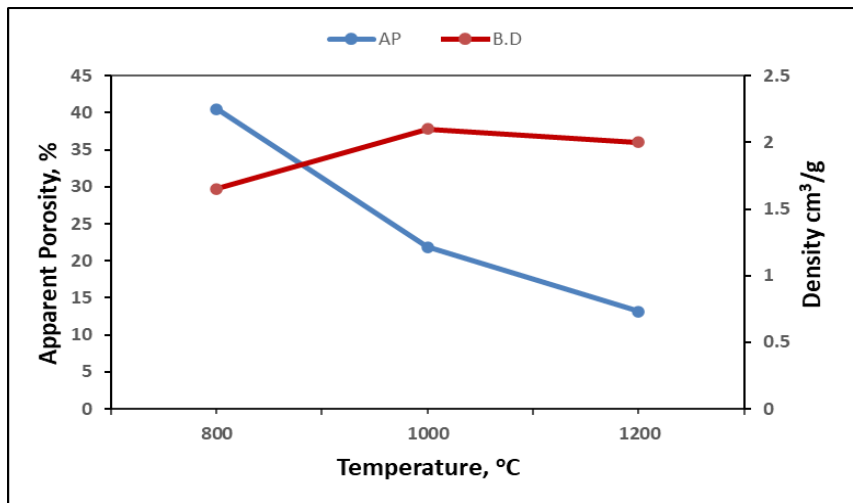


Fig. 3: The apparent porosity and bulk density of β -eucryptite ceramics sintered at 800, 1000 and 1200°C.

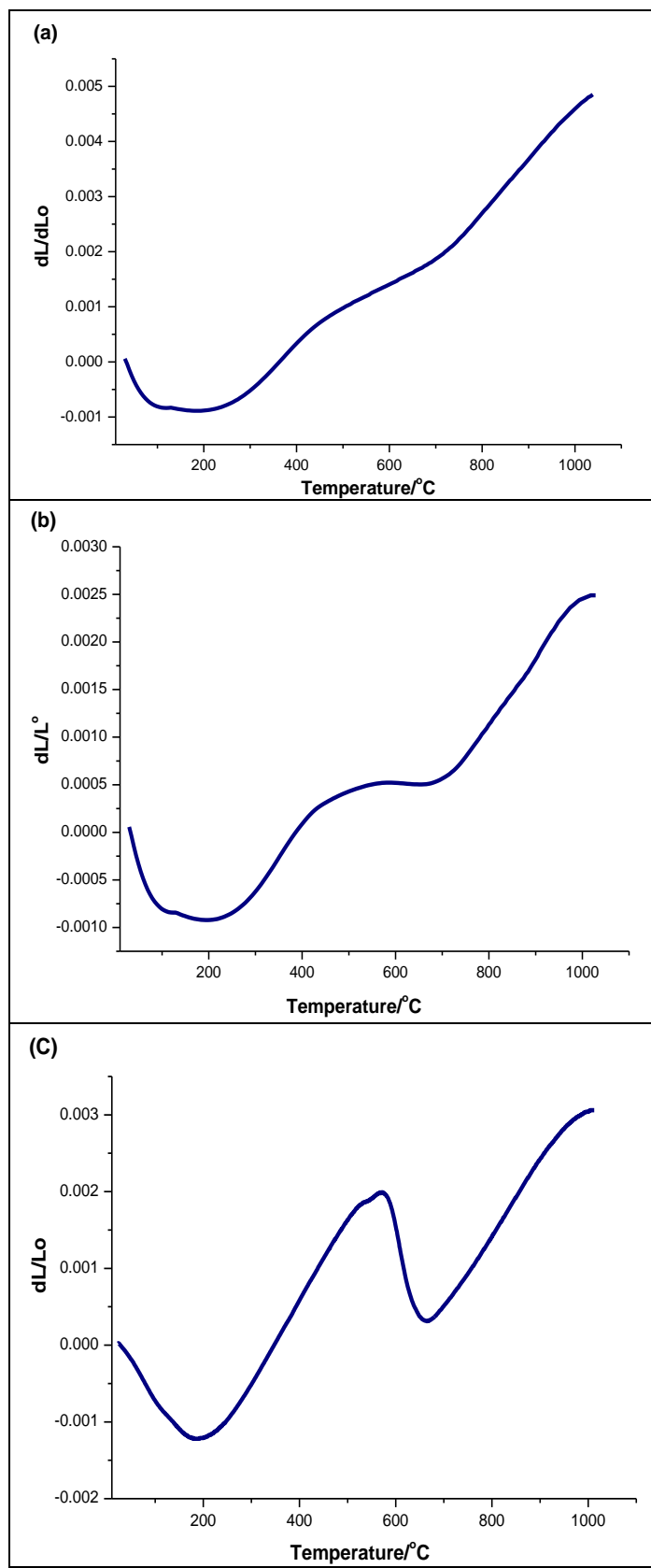


Fig. 4: Thermal expansion of β -eucryptite sintered at different temperatures: a) 800, b) 1000, and C) 1200 $^{\circ}\text{C}$.

Depending on the temperature, these structures may be occupied. At room temperature, the Li atoms are occupied in a tetrahedron structure. The possibility of Li atoms occupying an octahedral structure increases as temperature rises. At higher temperatures, Li atoms occupy some octahedral structures of β -eucryptite. When a Li atom occupies an octahedral structure, the (Si, Al) O_2 framework surrounding this site is influenced. The framework close to the Li atoms expands and contracts in a plane parallel to the a and c axes, respectively. With increasing temperature, the number of occupied octahedral structures increases, followed by an increase in the a axis and a decrease in the c axis. In addition, the sudden positive thermal expansion from 420 $^{\circ}\text{C}$ to 580 $^{\circ}\text{C}$ is due to a glass phase with positive volume expansion. The beta-eucryptite ceramics fired at 1000 $^{\circ}\text{C}$ exhibit a continuous decrease in thermal expansion due to the decrease of the glass phase. When compared to other samples, ceramic samples sintered at 1200 $^{\circ}\text{C}$ exhibit an increase in thermal expansion property over a whole measuring temperature range. This is due to the formation of spodumene. It is widely known that the thermal expansion coefficient ranges from $-8.6 \times 10^{-6} \text{ }^{\circ}\text{C}^{-1}$ for beta-eucryptite to $0.9 \times 10^{-6} \text{ }^{\circ}\text{C}^{-1}$ for beta-spodumene [61].

3.5. Phase composition of alumina / β -eucryptite samples

The phase compositions of sintered samples containing different amount of β -eucryptite from 10 to 40 Wt.% on the expense of alumina are shown in Figs. 5, 6, and 7. It can be seen that there was no reaction between the LAS phase and alumina, preventing the formation of third phases like mullite. In addition, the contents of β -eucryptite increase and alumina decrease by increasing the eucryptite contents. In addition, it is observed that for the samples containing high percentage of eucryptite of about 30 and 40 Wt.%, small traces of spodumene are observed. The most noticeable peaks were found at $\sim 26^{\circ}$, which were represented by the crystalline phases β -spodumene ($\text{LiAlSi}_2\text{O}_6$; ICDD: 00-035-0797) [62] or β -eucryptite (LiAlSiO_4 ; ICDD: 00-017-0533) [63]. For 30 and 40 Wt.% of the β -eucryptite contents, both crystalline phases appeared in the same position.

All samples exhibit a similar pattern of peak positions at position 20, 22.7, 28, 39, 47, 49 and 56 $^{\circ}$ regardless of the intensities that is refers to eucryptite or spodumene beside the main peak of 26 $^{\circ}$ of eucryptite or spodumene. However, the 22.7 $^{\circ}$ is indicated to the formation of β -spodumene beside the main peak of spodumene 26. However, the peak at 22.7 $^{\circ}$ is indicated to the presence of β spodumene beside β - eucryptite. The calcined alumina pattern exhibits great crystallinity and narrow, well-defined diffraction, which can be attributed to the hkl reflections associated with the JCPDS file 1-089-7717 of α - Al_2O_3 (corundum) [64].

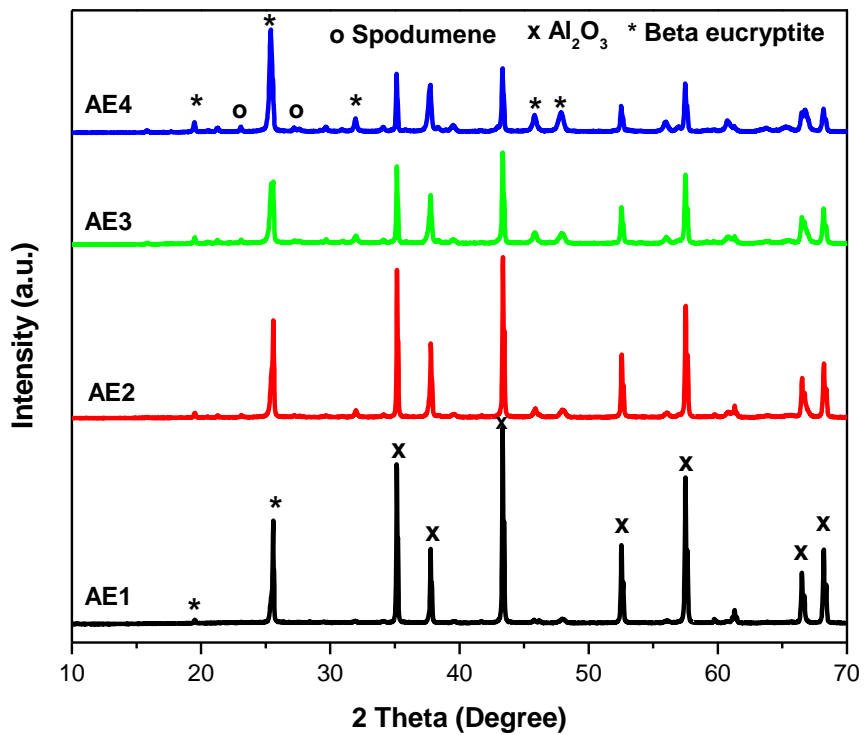


Fig. 5: XRD of the alumina/ β -eucryptite composites sintered at 1300°C

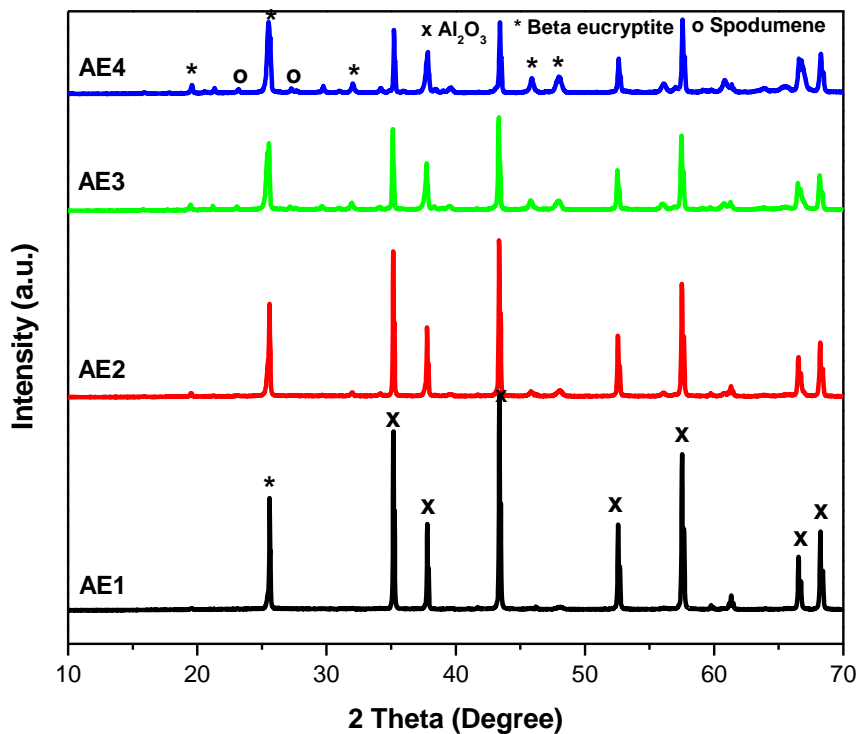


Fig. 6: XRD of the alumina/ β -eucryptite composites sintered at 1400°C

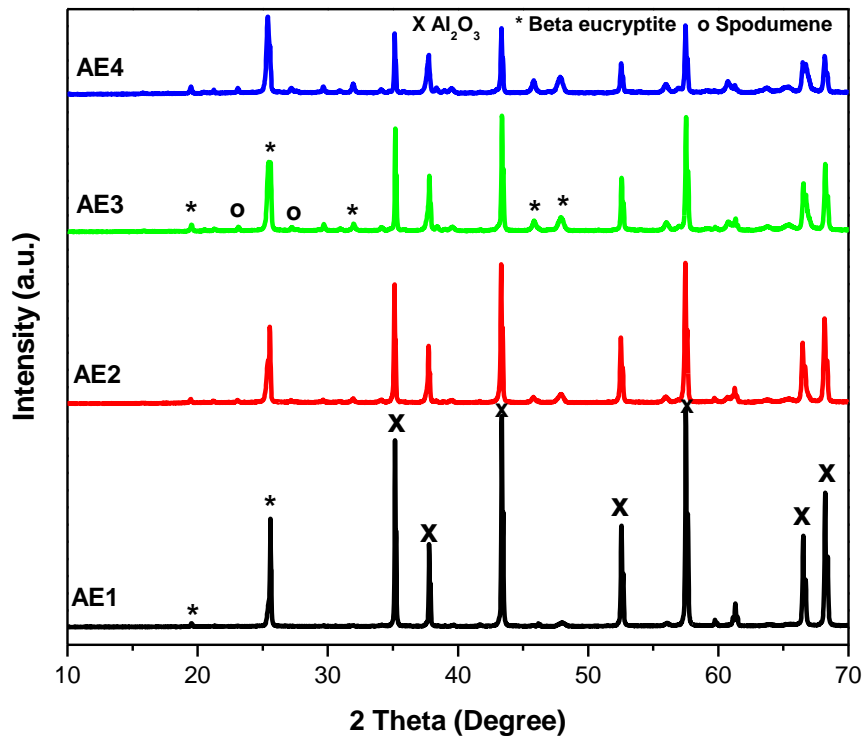


Fig.7: XRD of the alumina/ β -eucryptite composites sintered at 1500°C.

3.6. SEM of alumina / β -eucryptite samples

The SEM photographs of the microstructure of the alumina- alumina/ β -eucryptite composite at selected temperatures 1500°C are demonstrate in Fig. 8. The distribution of β -eucryptite particles within the alumina matrix can be observed. No cracks can be seen in SEM microstructure up to 30 Wt.% of β -eucryptite. The microstructures revealed by SEM images show porosity in the majority of the samples. Residual porosity is also seen, in agreement with the bulk density values obtained. The studied microstructures reveal that β -eucryptite is in rounded and tridimensional shapes with grain size in between 1 and 4 μm . The alumina appeared in hexagonal form, with a size range of 5-10 μm . The sub-micrometric LAS particles are embedded between alumina microns and are distributed uniformly as intra- and inter-granular particles, indicating β -eucryptite crystal growth during sintering. It was found that the increase in eucryptite content caused an increase in densification parameters due to the decrease in the viscous flow mechanism, allowing sintering to occur properly and be completely densified.

3.7 Physical properties

Figures 9, 10 illustrate the bulk density and apparent porosity of beta-eucryptite/alumina composites fired at 1300, 1400, and 1500°C with varying β -eucryptite concentration. It was observed the increase in eucryptite contents enhance the density and decrease the porosity up to 30 Wt.% of eucryptite. This is because in samples of alumina/ β -eucryptite, the grain boundary mobility in the Si-rich zone is greater than in the Al-rich zone. Similar to this,

sintering and grain boundary mobility may be facilitated by lithium-doped magnesium aluminate spinel [65-66].

According to the findings, increasing the β -eucryptite content to 30% wt and raising the sintering temperature increases bulk density while decreasing apparent porosity. This is because the solid-state reactions between the particles become stronger as the sintering temperature increases. At higher temperatures, densification was made easier thanks to the LAS materials' ability to form a liquid phase. Up to 1500°C, viscous flow, grain rearrangement, and glass redistribution are believed to be the main causes [65-66].

Figures 9 and 10 also demonstrate that the bodies' apparent porosity decreases with increasing sintering temperature and β -eucryptite concentrations to 30% at 1500°C. Bulk density is reported to decrease and apparent porosities increase for samples containing 40% by weight. This result is the result of the occurrence of microcracks and a trace amount of spodumene [53].

3.8. Mechanical strength

Figure 11 depicts the mechanical strength of alumina/ β -eucryptite composites sintered at various temperatures.

It was observed that that enhancement of strength with increasing the sintered temperature up to 1400°C. This is related to the porosity. As the decrease of apparent porosity enhance the mechanical behavior and deflect the crack propagation. Up increasing the sintered temperature up to 1500°C, the enhancement of the strength is observed up to 30 Wt.% eucryptite and reaches to maximum values of about 138 MPa. The strength values then start to decline. This might be because the

enlargement of β -eucryptite grain sizes (grain growth) and crack formations resulted in a decrease in density values and an increase in porosity values. It's important to note

that crack formation has a detrimental effect on the mechanical characteristics of burned ceramics [53].

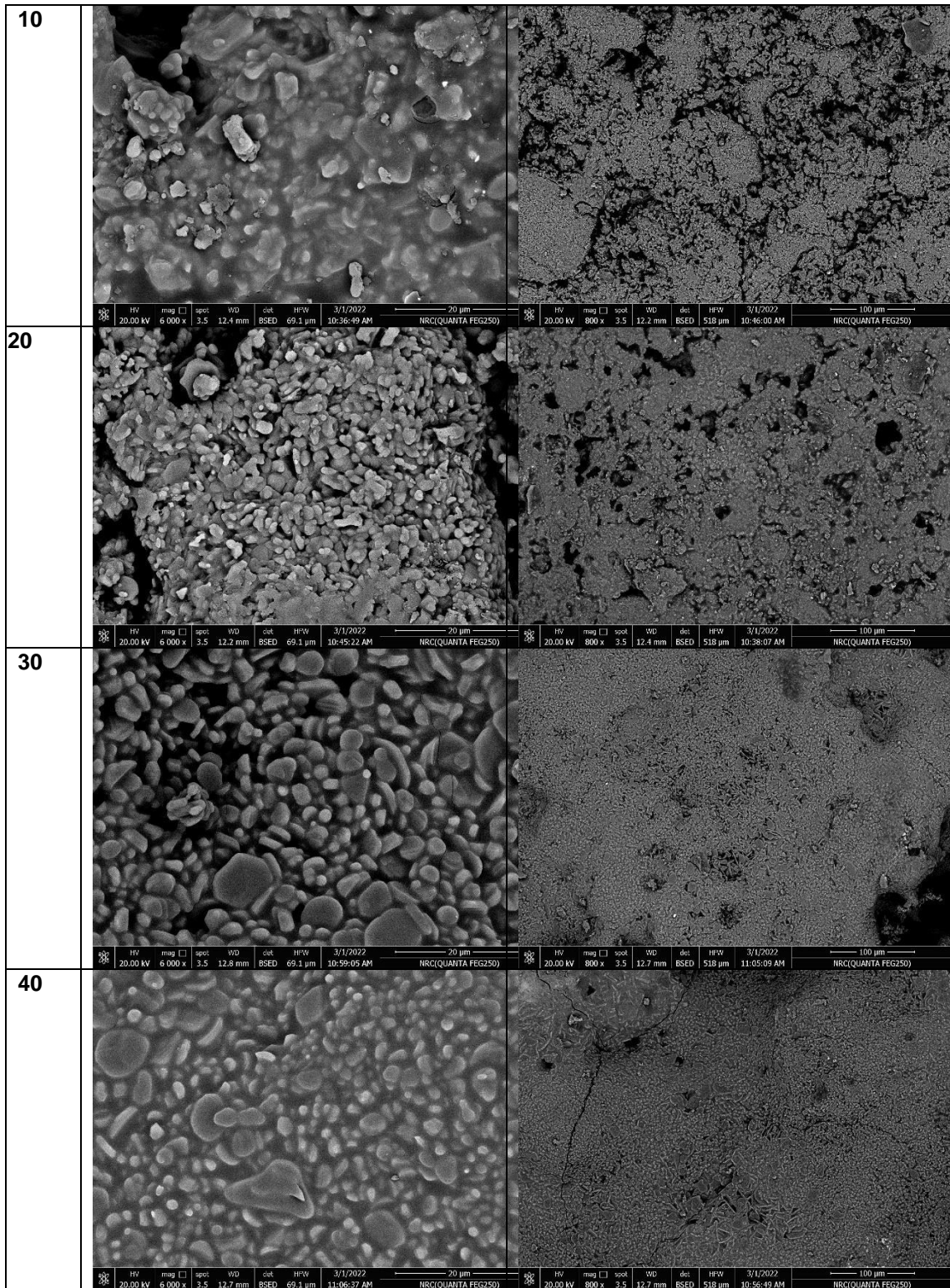


Fig. 8: The SEM photographs of alumina/ β -eucryptite composite sintered at 1500°C

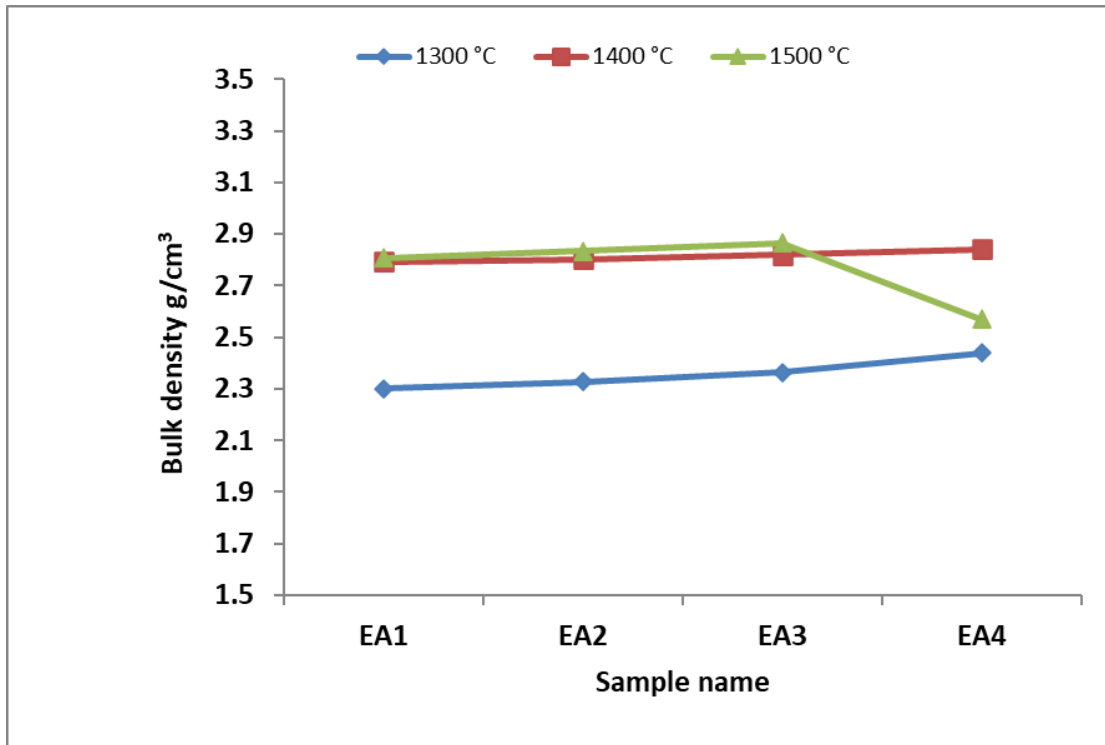


Fig. 9: The bulk density of alumina/ β -eucryptite composites sintered at 1300, 1400 and 1500°C

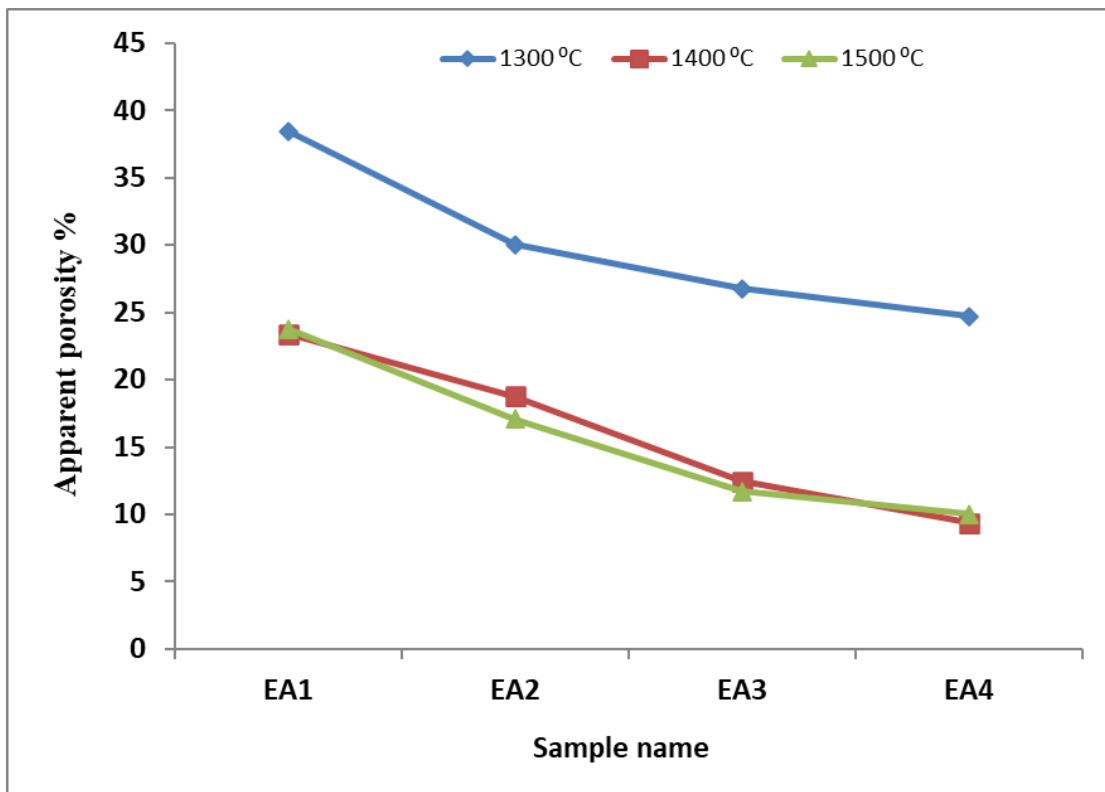


Fig. 10: The apparent porosity of alumina/ β -eucryptite composites sintered at 1300, 1400 and 1500°C.

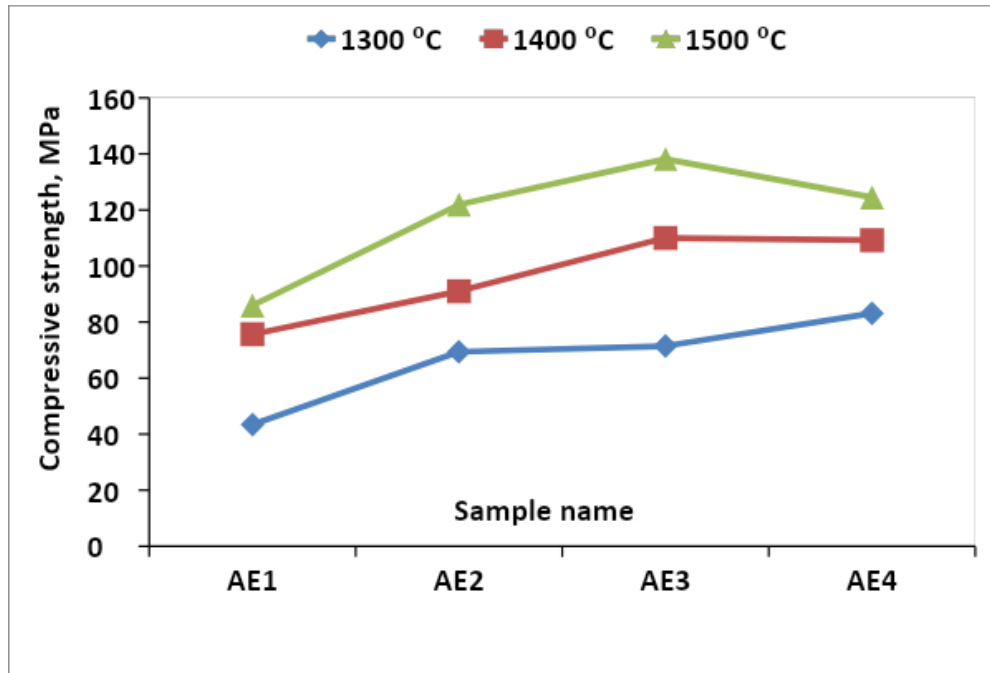


Fig. 11: Mechanical strength of alumina/β-eucryptite composites at different sintered temperatures.

3.9 Thermal expansion coefficient

Table 2 shows the coefficient of thermal expansion for various alumina/β-eucryptite samples at 1500°C sintering temperature. Because alumina and the LAS do not react, it is possible to predict the final phase composition and thus design many attributes into the material, including its CTE. The CTE value is determined by the composite's initial composition, body phases, and microstructure. The CTE of alumina/β-eucryptite composites reduces as the β-eucryptite content increases, as shown in Table 1, which is a feature of β-eucryptite behavior [67-70]. As is common knowledge, β-eucryptite has a thermal expansion coefficient of $-6.2 \times 10^{-6} \text{ } ^\circ\text{C}^{-1}$, whereas alumina has a thermal expansion coefficient of $10.3 \times 10^{-6} \text{ } ^\circ\text{C}^{-1}$ [71, 72]. The present of few amounts of spodumene does not effect on the trend of thermal expansion especially for sample contain 40 Wt.% of β-eucryptite, although thermal expansion of spodumene is about $0.9 \times 10^{-6} \text{ } ^\circ\text{C}^{-1}$ [73].

Table 2: Coefficient of thermal expansion for alumina/eucryptite composite at temperature 1500°C.

Composites	Al : Eu	Value of CTE x 10 ⁻⁶ °C ⁻¹
AE1	90 : 10	4.8658
AE2	80 : 20	3.2775
AE3	70 : 30	2.3456
AE4	60 : 40	0.8098

Conclusion

This work succeeded in the extraction of alumina from sludge waste to use it with a silica fume approach to make an alumina-eucryptite ceramic composite. In this work, the sinterability of an alumina/β-eucryptite composite is carried out at various temperatures: 1300, 1400, and 1500°C. The study's findings are as follows:

1. In composites containing a high percentage of eucryptite (between 30 and 40% by weight), small traces of spodumene are found. At 26°, the most prominent peaks were found, which were represented by crystalline phases of beta-eucryptite or beta-spodumene.
2. At 1500°C, the microstructure of the alumina/β-eucryptite composite revealed no cracks in up to 30% of the β-eucryptite samples.
3. With increasing β-eucryptite content up to 30% Wt.% at 1500°C, increasing the sintering temperature causes an increase in bulk density and a decrease in apparent porosity.
4. For samples containing 40% by weight, bulk density is reported to decrease while apparent porosities increase. This is due to the presence of microcracks and a trace amount of spodumene.
5. By increasing the sintered temperature up to 1500°C, the strength enhancement is observed up to 30 Wt.% eucryptite and reaches maximum values of about 138 MPa.
6. CTE of alumina/β-eucryptite composites decreases with increasing β-eucryptite content, reaching $0.8098 \times 10^{-6} \text{ } ^\circ\text{C}^{-1}$.

References

1. J. Lienig, H. Bruemmer, *Recycling Requirements and Design for Environmental Compliance: Fundamentals of Electronic Systems Design*, Springer International Publishing AG. (2017) 193-218.
2. M. Geissdoerfer, P. Savaget, N.M. Bocken, E.J. Hultink, The circular economy , A New Sustainability Paradigm, *Journal of Cleaner Production* . 143 (2017) 757-768.
3. SH. K. Amin, S.A. El-Sherbiny, H.H. Abo-Elmaged, M.F. Abadir, *Recycling of Marble Waste in the Manufacturing of Ceramic Roof Tiles*, *Global Waste Management*. (2017) 559-565.
4. A. H. Rania, E. Salah, K. Safwan, *Marble and Granite Waste: Characterization and Utilization in Concrete Bricks*, *International Journal of Bioscience, Biochemistry and Bioinformatics*. 1, 4 (2011) 286-290.
5. R. A. Barakwan, Y. Trihadiningrum, A. Y. Bagastyo, *Characterization of Alum Sludge from Surabaya Water Treatment Plant*, *Journal of Ecological Engineering*. 20 (5) (2019) 7-13
6. M. H. Hassan Basri, N. N. Mohammad Don, N. Kasmuri , N. Hamzah , S. Alias, F. A. Azizan , *Aluminum Recovery from Water Treatment Sludge under Different Dosage of Sulphuric Acid*, *Journal of Physics: Conference Series*. 1349(2019) 012005 doi:10.1088/1742-6596/1349/1/012005
7. K. Fytianos, E. Voudrias, N. Raikos, *Modeling of Phosphorus Removal from Aqueous and Wastewater Samples Using Ferric Iron*. *Environmental Pollution*. 101 (1998)123-130.
8. R. B. Sotero-Santos , O. Rocha , J. Povinelli , *Toxicity of Ferric Chloride Sludge to Aquatic Organisms*. *Chemosphere*. 68(2007) 628 -636.
9. C. H. Wu, C. F. Lin, W. R. Chen. *Regeneration and Reuse of Water Treatment Plant Sludge: Adsorbent for Cations*. *Journal of Environmental Science and Health, Part A* 39 (3) (2004)717-728.
10. I. Ali. *The Quest for Active Carbon Adsorbent Substitutes: Inexpensive Adsorbents for Toxic Metal Ions Removal from Waste Water*. *Separation & Purification Methods* 39 (3-4) (2010) 95-171.
11. M.B. Sedelnikova, N.V. Liseenko, Y.I. Pautova, V.M. Pogrebenkov, *Heat-Resistant Ceramic Pigments on the Base of Waste Vanadium Catalyst and Alumina* *Journal of Waste Management*. 369174 (2013) 6
12. Y.M. Abu-Ayana, E.A.M. Yossef, S. M. El-Sawy, *Silica Fume – Formed During the Manufacture of Ferrosilicon Alloys– As An Extender Pigment in Anticorrosive Paints*, *Anti-Corrosion Methods and Materials*. 52 (3) (2005) 345-352.
13. J.E. Alleman, *Beneficial Use of Sludge in Building Components. Concept Review and Technical Background*. *Interbrick*. 3(2) (1987) 14-20.
14. J. Danie, MD. Berry, M.D. Jay Lieberman, in *Surgery of the Hip*, Elsevier, 2nd. Edition 3(5), September 24, 2019.
15. C. Piconi , *Comprehensive Biomaterials II*, Elsevier, Volume 1, 2017, Pages 92-121.
16. A. Mehtaa, D. K. Ashish, *Silica Fume and Waste Glass in Cement Concrete Production: A review*, *Journal of Building Engineering*. 29 (2020) 100888.
17. R. Siddique, *Utilization of Silica Fume in Concrete: Review of Hardened Properties, Resources, Conservation and Recycling*.55 (2011) 923-932.
18. R.M. Khattab, H.A. Badr, H.H. Abo-Elmaged, H.E.H. Sadek, *Recycling of Alum Sludge for Alpha Al₂O₃ Production using Different Chemical Treatments, Desalination and Water Treatment*. 113 (2018) 148-159.
19. L. Xia, G.W. Wen, C.L. Qin, X.Y. Wang, L. Song, *Mechanical and Thermal Expansion Properties of β -eucryptite Prepared by Sol-Gel Methods and Hot Pressing*, *Materials and Design*. 32 (2011) 2526-2531.
20. O.V. Kichkailo, I.A. Levitskii, *Lithium-Bearing Heat-Resistant Ceramics (A Review)*, *Glass and Ceramics*. 62 (2005) 5-6.
21. G.N. Maslennikova, F.Ya . Kharitonov, *Electroceramics Resistant to Thermal Shocks in Russian*, *Énergiya, Moscow*, (1977).
22. F.C. Campbell, R .Steven. Lampman, *Structural Composite Materials*, New York. (2003) 40-43.
23. M.A. Saleh, S.M. Naga, M. Awaad, A.I. Faïd , Y.I. , *El-Shaer Synthesis and Characterization of Alumina-Spodumene Ceramic Composites*, *aerospace science & aviation technologist*. 13, May (2009) 26-28.
24. O. García-Moreno, A. Borrell, B. Bittmann, A. Fernández, R. Torrecillas, *Alumina Reinforced Eucryptite Ceramics: Very Low Thermal Expansion Material with Improved Mechanical Properties*, *Journal of the European Ceramic. Society* .31 (2011) 1641-1648.
25. M. Oghbaei, O. Mirzaee, *Microwave Versus Conventional Sintering. A Review of Fundamentals, Advantages and Applications*, *J. Alloy. Comp*. 494 (2010) 175-189.
26. K.I. Rybakov, E.A. Olevsky, E.V. Krikun, *Microwave sintering: Fundamentals and Modeling*, *Journal of the American Ceramic Society*. 96(4) (2013) 1003-1020.
27. M. Mizuro, S. Obata, S. Takayama, S. Ito, N. Kato, T. Hiraia, M. Sato, *Sintering of Alumina by 2.45 GHz Microwave Heating*, *Journal of European Ceramic Society*, 24 (2004) 387-391.
28. R. Benavente, M.D. Salvador, F.L. Peñaranda-Foix, E. Pallone, A. Borrell, *Mechanical Properties and Microstructural Evolution of Alumina-Zirconia Nanocomposites by Microwave Sintering*, *Ceramic International*. 40 (2014) 11291-11297.
29. R. Benavente, A. Borrell, M.D. Salvador, O. García-Moreno, F.L. Peñaranda-Foix, J.M. Catala-Civera, *Fabrication of Near-Zero Thermal Expansion of Fully Dense β -eucryptite Ceramics by Microwave Sintering*, *Ceramic International*. 40 (2014) 935-941.
30. J.P. Cheng, D.K. Agrawal, S. Komameni, M. Mathis, R. Roy, *Microwave Processing of WC-Co Composites and Ferroic Titates*, *Material Research Innovations*. 1(1997) 4-52.
31. Y. Fang, D.K. Agrawal, R. Roy, *Fabrication of Transparent Hydroxyapatite Ceramics by Ambient-Pressure Sintering*, *Material Letters*. 23 (1995) 147-151.
32. J. Cheng, D. Agrawal, Y.Zhang, R. Roy, *Microwave Sintering of Transparent Alumina*, *Material Letters*. 56 (2002) 587-592.
33. R.M. Khattab, H.E.H. Sadek, F. Abd-EL-Raouf, H.A. Badra, H.H. Abo-Elmaged *Effect of Alkali Roasting and Sulfatization on the Extraction of Different Metal Oxides from Waste Alum Sludge*, *Ceramic International*. 47 (16) (2021) 23181-23193.
34. O. García-Moreno, A. Fernández, R. Torrecillas, *Solid State Sintering of Very Low and Negative Thermal Expansion Ceramics by Spark Plasma Sintering*, *Ceramic International*. 37 (2011) 1079-1083.
35. O. García-Moreno, A. Fernández, R. Torrecillas, *Sintering of Mullite- β -Eucryptite Ceramics with Very Low Thermal Expansion*, *International Journal of Material Research*. 103 (2012) 416-421.
36. Z. Li-Min, C. Yong-Guang, H. Hao-Shan, W. Jiao, L. Shao-Hui, Z. Bao-Sen, *Properties of Negative Thermal Expansion β -*

- eucryptite Ceramics Prepared by Spark Plasma Sintering, *Physics B*. 27(9) (2018) 096501.
37. L. Husniyah Aliyah, B.M. Izzat1, M. Hasmaliza1, A. Tuti Katrina1, Effect of mechanical properties on sintered lithium alumino- silicate glass ceramic and its thermal shock resistance properties *AIP Conference Proceedings*. 2267 (2020) 020047.
38. J. Zhan, Y. Long, Synthesis of Bi₂Mn₄O₁₀ Nanoparticles and Its Anode Properties for LIB. *Ceramic International*, 44(12) (2018)14896-14900.
39. P. Lu, Y. Zheng, J. Cheng, and D. Guo, Effect of La₂O₃ Addition on Crystallization and Properties of Li₂O–Al₂O₃-SiO₂ Glass-Ceramics. *Ceramic International*. 39(7) (2013) 8207-8212.
40. T. Yang and S. Liu, Hong. Ju. Zhai, Li. Jing. Wang, Dong. Lai. Han, Huan. Wang, Jian . Wang, Xiao. Yan. Liu, Xue. Lin ,Xiu .Yan. Li , Ming. Gao, Jing. Hai. Yang, Facile One-Step Synthesis and Photoluminescence Properties of Ag–ZnO Core–Shell Structure. *Journal of Alloys and Compounds*. 600 (2014) 51-54.
41. E. Kleebusch, C. Patzig, T. Höche, C. Rüssel, The Evidence of Phase Separation Droplets in the Crystallization Process of a Li₂O-Al₂O₃-SiO₂ Glass with TiO₂ as Nucleating Agent- An X-ray Diffraction and (S)TEM-Study Supported by EDX-Analysis. *Ceramic International*. 44 (2018) 2919-2926.
42. S. Barbi, P. Miselli, and C. Siligardi, Failure Analysis of Glazed LAS Glass-Ceramic Containing Cerium Oxide. *Ceramic International*. 43 (2017) 1472-1478.
43. S. Arcaro, B. Moreno, E. Chinarro, M.D. Salvador, A. Borrell, M.I. Nieto, R. Moreno, A.P. Novaes de Oliveira, Properties of LZS/NanoAl₂O₃ Glass-Ceramic Composites. *Journal of Alloys and Compounds*. 710 (2017) 567-574.
44. A. Kumar, A. Chakrabarti, M. S. Shekhawat, and A. R. Molla, Transparent Ultra-Low Expansion Lithium Alumino-silicate Glass-Ceramics: Crystallization Kinetics, Structural and Optical Properties. *Thermochimica. Acta*. 676 (2019) 155-163.
45. M. Guedes, A.C. Ferro, and J.M.F. Ferreira, Nucleation and Crystal Growth in Commercial LAS Compositions. *Journal of the European Ceramic Society*. 21 (2001) 1187-1194.
46. F.C. Figueira and A.M. Bernardin, Sinter-crystallization of Spodumene LAS Glass-ceramic Tiles Processed by Single-Firing. *J. Alloys Compound*. 800 (2019) 525-531.
47. M.X. Gan and C.H. Wong, Properties of Selective Laser Melted Spodumene Glass-ceramic. *Journal of the European Ceramic Society*. 37(13) (2017) 4147-4154.
48. V.O. Soares, R.C.V. M. Reis, E.D. Zanotto, M.J. Pascual, and A. Durán, Non-isothermal sinter-crystallization of jagged Li₂O-Al₂O₃-SiO₂ Glass and Simulation using a Modified Form of the Clusters Model. *Journal of Non-Crystalline Solids*. 358 (23) (2012) 3234–3242.
49. D. Feng, Y. Zhu, F. Li, and Z. Li, Influence Investigation of CaF₂ on the LAS Based Glass-Ceramics and the Glass-Ceramic/diamond Composites. *Journal of the European Ceramic Society*. 36(10) (2016) 2579-2585.
50. Z. Qing, B. Li, H. Li, Y. Li, and S. Zhang, Effects of MgO on Properties of Li₂O–Al₂O₃–SiO₂ Glass–ceramics for LTCC Applications. *Journal of Materials Science Mater Electron*. 25 (5) (2014) 2149-2154.
51. P. Rielloa, S. Bucellaa, L. Zamengoa, U. Anselmi-Tamburini, R. Francinic, S. Pietrantonio, Z.A. Munir, Erbium-doped LAS Glass Ceramics Prepared by Spark Plasma Sintering (SPS). *Journal of the European Ceramic Society*. 26 (15) (2006) 3301–3306.
52. W. Gong, H. Li, L. Wang, E. Wang, Pressureless Sintering and Mechanical Properties of 3Y-TZP-reinforced LZAS Glass-Ceramic Composites. *Ceramic International*. 42(16) (2016) 18053–18057.
53. R.M. Khattab a, H.E.H. Sadek, A. Mohammed Taha, Amira M. EL-Rafei, Recycling of Silica Fume Waste in the Manufacture of β-eucryptite Ceramics Materials Characterization. 171 (2021) 110740.
54. Y. Tang, Q. Zhang, Z. Luo, P. Liu, and A. Lu, Effects of Li₂O-Al₂O₃-SiO₂ System Glass on the Microstructure and Ionic Conductivity of Li₇La₃Zr₂O₁₂ Solid. *Electrolyte Material Letters*. 193 (2017) 251-254.
55. C.G. Shi, I.M. Low, Effect of Spodumene Addition on the Sintering and Densification of Aluminum Titanate. *Materials Research Bulletin*. 33 (6) (1998) 817-824.
56. I.M. Low, P.M. Suherman, D.N. Phillips, Synthesis and Properties of Spodumene-Modified Mullite Ceramics Formed by Sol-Gel Processing. *Journal of Material Science Letters*. 16 (1997) 982-984.
57. H. Kobayashi, N. Ishibashi, T. Akiba, T. Mitamura, Preparation and Thermal Expansion of Mullite-β-Spodumene Composite. *Journal of Ceramic Society Japan*. 98 (1990) 1023-1028 .
58. R.D. SARNO, M. Tomozawa, Toughening Mechanisms for a Zirconia-Lithium Alumino-silicate Glass-ceramic, *Journal of Materials Science*. 30 (1995) 4380-4388.
59. K. Takenaka, Negative Thermal Expansion Materials: Technological Key for Control of Thermal Expansion, *Science Technology of Advanced Materials*. 13 (2012) 013001.
60. H. Schulz, Thermal Expansion of β-eucryptite. *Journal of American Ceramic Society*. 57 (1974) 313.
61. Li-Min Zhao, Yong-Guang Cheng, Hao-Shan Hao, Jiao Wang, Shao-Hui Liu, Bao- Sen Zhang, Properties of Negative Thermal Expansion β-eucryptite Ceramics Prepared by Spark Plasma Sintering. *Chinese Physics B*. 27 (9) (2018) 096501.
62. R. Roy, D.M. Roy, E.F. Osborn, Compositional and Stability Relationships Among the Lithium Alumino-silicates: Eucryptite, Spodumene and Petalite. *Journal of the American Ceramic Society*. 33 (5) (1950) 152-159.
63. K.H. Kim, F.A. Hummel, Studies in Lithium Oxide Systems: IX Li₂O–Al₂O₃–TiO₂. *Journal of the American Ceramic Society* 43 (12) (1960) 611-614.
64. F.Y. Galakhov. Alumina Region of Ternary Alumino-silicate Systems Communication 4. The System Li₂O–Al₂O₃–SiO₂. *Bull Academy of Science of USSR. Division of Chemistry Science*. 8 (4) (1959) 550-556.
65. J.A. Geodakyan, A.K. Kostanyan, K.J. Geodakyan, S.T. Sagatelyan, B.V. Petrosyan, The Influence of β-eucryptite Glass Ceramics on the Structure and Main Properties of Alumina Ceramics. In: 28th. International Conference on Advanced Ceramics and Composites. (2004).
66. S.M. Naga, A.A. El-Maghraby, H. Mörtel, Densification and Characterization of β-spodumene–cordierite compositions. *The American Ceramic Society. Bull.* 85 (11) (2006) 9101-U10.
67. S. Mandal, S. Chakrabarti, S. Das, S. Ghatak, Sintering Characteristics of in-Situ Formed Low Expansion Ceramics from A Powder Precursor in the Form of Hydroxy hydrogel. *Ceramic International*. 30 (2004) 2147- 2155.
68. R. Benavente, A. Borrell , M.D. Salvador, O.G. Moreno, F. Penaranda-Foix, J.M. Catalá-Civera, Fabrication of Near-zero

Thermal Expansion of Fully Dense β -eucryptite Ceramics by Microwave Sintering. *Ceramic International*. 40 (2014) 935-941.

69. E. Breval , H. A. McKinstry , D. K. Agrawal , New [NZP] materials for protection coatings, Tailoring of thermal expansion, *Journal of Materials Science* 35 (13) (2000) 3359-3364.

70. L. Xia, G. W. Wen, L. Song, X.Y. Wang. The Crystallization behavior and Thermal Expansion Properties of β -eucryptite Prepared by Sol-Gel Route. *Materials Chemistry and Physics*. 119 (2010) 495-498.

71. P. Zhai, X. Duan, D. Chen, C. Wang, Preparation and Characterization of β -eucryptite Glass Ceramics. *Advanced of Material Researches*. 624 (2013) 134-137.

72. H.H. Abo-Elmagd, W.H. Hegazy , M.E.M. Sebak , R.M. Khattab, The Effect of Temperature on Synthetic Nano β -eucryptite and Alumina Ceramic Materials: Thermal Expansion, Mechanical, and Physical Properties. *Silicon* (2022), 1-15.

73. L.H. Aliyah , B.M. Izzat , M. Hasmaliza , A.T. Katrina, Effect of Mechanical Properties on Sintered Lithium Alumino-silicate Glass Ceramic and its Thermal Shock Resistance Properties, 3rd. International Postgraduate Conference on Materials, Minerals and Polymer (MAMIP), (2019).